Two-stage intelligent planning with improved artificial bee colony algorithm for a microgrid by considering the uncertainty of renewable sources

Saeed, Muhammad Hammad; Fangzong, Wang; Salem, Sultan; Khan, Yousaf Ali; Kalwar, Basheer Ahmad; Fars, Ashk

DOI:
10.1016/j.egyr.2021.10.123

Energy Reports 7 (2021) 8912–8928

Contents lists available at ScienceDirect

Energy Reports

journal homepage: www.elsevier.com/locate/egyr

Research paper

Two-stage intelligent planning with improved artificial bee colony algorithm for a microgrid by considering the uncertainty of renewable sources

Muhammad Hammad Saeed [a,*], Wang Fangzong [a], Sultan Salem [b,**], Yousaf Ali Khan [c], Basheer Ahmad Kalwar [a], Ashk Fars [d]

[a] Research Centre for Microgrid of New Energy, College of Electrical Engineering and New Energy, China Three Gorges University, 8 Daxue Road, Xiling District, Yichang 443002, Hubei, P.R. China
[b] Department of Economics, Birmingham Business School (BBS), University of Birmingham, United Kingdom
[c] Department of Mathematics and Statistics, Hazara University Mansehra, 23010, Pakistan
[d] Electrical and Electronic Engineering Department, Sunlife Company, Baku, Azerbaijan

ARTICLE INFO

Article history:
Received 13 July 2021
Received in revised form 12 October 2021
Accepted 31 October 2021
Available online 3 December 2021

Keywords:
Optimization
Microgrid planning
Renewable resources
Artificial bee colony algorithm

ABSTRACT

A two-stage planning form of multi-energy supply optimization such as power, cooling, and heating is presented in this paper as a micro energy grid (MEG) To cover the effect of uncertainty in renewable energy sources (RES), the scheduling cycle is considered in this paper. Next, the results of the day-ahead prediction are considered as random variables for the upper-layer model. To realize the random variables at the lower layer, the revised model of energy storage and the demand response (DR) planning model are considered. Finally, the modified version of the artificial bee colony (ABC) algorithm is utilized to find the optimal solution. The improved ABC algorithm is a shape-memory method based on the collective intelligence and behavior of bees in a colony for finding the best nutrition source. In the improved ABC algorithm, with information exchange between the bees, based on Newton's law of universal gravitation, the full potential of this algorithm is used to find the optimal solution given the constraints applied to the system. The proposed method is applied to a real system and the results show that the two-stage optimization algorithm and the proposed intelligent algorithm obtained the simultaneous optimization of different energy forms. The obtained numerical analysis results in test cases prove the following points: (1) The optimal synergistic supply of multiple energy forms has been provided based on the two-stage optimization algorithm and solution approach. (2) The surplus energy can be converted to natural gas by the power-to-gas converter (P2G) based on power cascade conversion in a multi-directional mode. (3) To get some revenue, the MEG is flexible enough to cooperate with the upper-grade energy network. (4) The DR-based price can smooth the load shape and increase the MEG operation revenue using some supplementary features. Also, P2G can sequentially develop the flexible multidirectional energy conversion in energy - gas - energy - cooling as a cascade. When the evaluated P2G energy rises by 450 kW, the total GST output raises by 1244 kWh. For more economic benefits, MEG can be connected to the upstream energy grid. Load management also increases the net revenue of the system.

1. Introduction

Considering the worldwide concerns about environmental emissions, the inflexibility of traditional methods of energy supplement poses some problems in gathering the desires for economic and social progress. The energy distribution network systems, with clean energy as the main energy resource, have received more attention recently. In 2011, Jeremy Rifkin, an American researcher, proposed the first view on the Internet of Energy in the third industrial revolution. As a normal microgrid (MG)

* Correspondence to: Research Center for Microgrid of New Energy, College of Electrical Engineering and New Energy, China Three Gorges University, Hubei, Yichang, P.R. China.
** Correspondence to: Birmingham Business School (BBS), University of Birmingham, United kingdom.
E-mail addresses: muhammad005@ctgu.edu.cn (M.H. Saeed), s.salem@bham.ac.uk (S. Salem).

https://doi.org/10.1016/j.egyr.2021.10.123

Nomenclature

MEG	Micro energy grid
EP	Energy production
WPP	Wind power plant
PV	Photovoltaic
CGT	Convention gas turbine
GB	Gas boiler
EC	Energy conversion
P2H	Power to heating
P2C	Power to cooling
P2G	Power to gas
H2C	Heating to cooling
ES	Energy storage
PS	Power storage
GS	Gas storage
HS	Heating storage
CS	Cooling storage
PBDR	Price-based demand response
IBDR	Incentive-based demand response
PSO	Particle swarm optimization

Set

s,t	Index for time
j	Index for probability
e	Index for electricity
h	Index for heating
c	Index for cooling

Parameter

v_{in}	Cut-in speed
v_{out}	Cut-out speed
v_{rated}	Rated speed
η_{pv}	Operation efficiency
S_{PV}	Area of photovoltaic panels
η_{hr}	Heating recovery efficiency of CGT
H_{ng}	Calorific value of natural gas
$Q_{\mathrm{P2H},t}$	Heating output of P2H at time t
$Q_{\mathrm{H2C},t}$	Cooling output of H2C at time t
$g_{\mathrm{P2C},t}$	Power consumption of P2H at time t
$g_{\mathrm{P2H},t}$	Power consumption of P2C at time t
$Q_{\mathrm{H2C},t}$	Heating consumption of H2C at time t
$V_{GS,t}^{P2G}$	Natural gas into GS produced by P2G at time t
η_{GB}	Heating efficiency of GB
η_{P2G}	Conversion efficiency of P2G
η_{P2C}	Efficiency of P2C
η_{P2H}	Efficiency of P2H
η_{H2C}	Efficiency of H2C
$S_{\mathrm{GS,T0}}$	Storage energy of GS at initial time
θ_{h}	Heating-power conversion coefficient
a_i, b_i, c_i	Cost coefficients of CGT power generation
φ_{GT}	Power consumption rate of CGT
$P_t^{(e,h,c)0}$	Prices of power, heating and cooling before PBDR at time t
$c_{\min}$	Coefficients under the minimum power generation output
$\mu_{\blacksquare}$	Social learning factor of low-concentration subgroups

Variables

$g_{WPP,t}^{*}$	Available power output of WPP at time t
v_t	Natural wind speed at time t
$g_{PV,t}^{*}$	Available output of PV at time t
θ_{t}	Solar radiation intensity at time t
$g_{CGT,t}$	Power output of CGT at time t
$Q_{CGT,t}$	Heating output of CGT at time t
$V_{CGT,t}$	Natural gas consumption of CGT at time t
$\eta_{CGT,t}$	Power generation efficiency of CGT at time t
$E_{EC,t}^{out}$	Energy supply at time t
$P_{EC,t}^{out}$	Energy consumption price of EC at time t
$E_{EC,t}^{in}$	Energy quantity of EC at time t
$\varphi_{EC,t}^{out}$	Efficiency of outputting energy of EC at time t
$\varphi_{EC,t}^{in}$	Efficiency of inputting energy of EC at time t
$\mathbf{R}_{\boldsymbol{ES},t}$	Revenue of ES at time t
$R_{PS,t}$	Revenue of power storage at time t
$R_{GS,t}$	Revenue of gas storage at time t
$R_{HS,t}$	Revenue of heating storage at time t
$R_{CS,t}$	Revenue of cooling storage at time t
$P_{ES,t}^{dis}$	Energy release price at time t
$P_{ES,t}^{ch}$	Energy storage price at time t
$g_{UG,t}$	Power supply of public grid at time t
$g_{\boldsymbol{RE},t}$	Power output of clean energy at time t
Q_t^{e}	Load demand of power at time t
Q_t^{h}	Load demand of heating at time t
Q_t^{c}	Load demand of cooling at time t
$\Delta\ Q^{\mathrm{PB},e\,t}$	Output of power from PBDR at time t
$\Delta\ Q^{\mathrm{PB},h\,t}$	Output of heating from PBDR at time t
$\Delta Q^{PB,c\,t}$	Output of cooling from PBDR at time t
ΔQ_s	Variations in demand after PBDR at time t
ΔP_t	Variations in price after PBDR at time t
$\Delta Q_t^{\mathrm{PB},(e,h,c)}$	Load variation after PBDR at time t
$Q^{e,h,c\,t}$	Initial load before PBDR at time t
$c_{\max}$	Coefficients under the maximum power generation output
Q_{CGT}^{max}	Maximum heating output
Q_{CGT}^{min}	Heating output of CGT when the generating power is minimum
g_{CGT}^{min}	Minimum power output of CGT under pure condensation condition
g_{CGT}^{max}	Maximum power output of CGT under pure condensation condition
$Q_{CGT,t}^{min}$	Minimum heating output of CGT at time t
$V_{P2G,t}^{min}$	Minimum gas generation of P2G at time t
$V_{P2G,t}^{max}$	Maximum gas generation of P2G at time t
$E_{EC,t}^{out,min}$	Minimum energy supply of EC at time t

$E_{EC,t}^{out,max}$	Maximum energy supply of EC at time t
$E_{EC,t}^{in,min}$	Minimum energy consumption of EC at time t
$E_{EC,t}^{in,max}$	Maximum energy consumption of EC at time t
$Q_{ES,t}^{ch,min}$	Minimum energy storage power at time t
$Q_{ES,t}^{ch,max}$	Maximum energy storage power at time t
$Q_{ES,t}^{dis,min}$	Minimum energy release power at time t
$Q_{ES,t}^{dis,max}$	Maximum energy release power at time t
$S_{ES,t}^{min}$	Minimum energy storage at time t
$S_{ES,t}^{max}$	Maximum energy storage at time t
$V_{GS,t}^{P2G,min}$	Minimum gas generation of GS at time t
$V_{GS,t}^{P2G,max}$	Maximum gas generation of GS at time t
T_0	Beginning of the scheduling cycle
T	End of the scheduling cycle
$g_{MEG,t}^{max}$	Maximum power output of MEG at time t
$g_{MEG,t}^{min}$	Minimum power output of MEG at time t
r^e	Reserved coefficients of loads
r_{WPP}	reserved coefficients of WPP
r_{PV}	Reserved coefficients of PV
r	Concentration dividing radius, usually the value is 0.4∼0.6
K	Total iterative evolution number of particles
J	Number of low-concentration particle swarm
k	Particle dimension
μ_1	social learning factor of whole particle swarm
η_{loss}	power loss rate
μ_2	Social learning factor of low-concentration subgroup
ϕ	State quantity
$Q_{GB,t}$	Heating output of GB at time t
$V_{GB,t}$	Gas consumption of GB at time t
$V_{\mathrm{P2G},t}$	CH_4 Generated by P2G at time t
$g_{\mathrm{P2G},t}$	Power consumption by P2G at time t
$Q_{\mathrm{P2C},t}$	Cooling output of P2C at time t
$\eta_{P2G,t}^{loss}$	Gas loss rate at time t
$S_{\mathrm{GS},t}$	Storage energy of GS at time$t$
$V_{GS,t}^{GB}$	Natural gas from GS to GB at time t
$V_{GS,t}^{NG}$	Natural gas from GS to gas network at time t
$Q_{ES,t}$	Net energy output of ES devices at time t
$Q_{ES,t}^{ch}$	Energy of ES storing at time t
$Q_{ES,t}^{dis}$	Energy of ES releasing at time t
$u_{ES,t}^{ch}$	State variables of ES storing
$u_{ES,t}^{dis}$	State variables of ES releasing
$S_{ES,t}$	Stored energy at time t

η_t^{loss}	Energy loss rate at time t
$\varphi_{ES,t}^{ch}$	Energy efficiency of ES storing at time t
$\varphi_{ES,t}^{dis}$	Energy efficiency of ES releasing at time t
$P_{CGT,t}^{e}$	Prices of power provided by CGT at time t
$P_{CGT,t}^{h}$	Prices of heating provided by CGT at time t
$P_{ng,t}$	Natural gas price at time t
$\mu_{CHP,t}^{u}$, μ_C^d	Operation status of CGT at time t, 0-1 variables
$C_{CGT,t}^{u}$	Start cost of CGT at times t
$C_{CGT,s+1}^{d}$	Stop cost of CGT at times $s+1$
$R_{EC,1}$	Operation revenue of EC at time t
$P_{EC,t}^{out}$	Energy supply price at time t
$\pi_t^{IB,(e,h,c)}$	Cost of power, heating and cooling of IBDR at time t
$\Delta Q_{IB,t}^{E}$	Output of IBDR in energy scheduling market at time t
$\Delta Q_{IB,t}^{up}$	Upper reserved output of IBDR in reserved scheduling market at time t.
$\Delta Q_{IB,t}^{dn}$	Down reserved output of IBDR in reserved scheduling market at time t.
$\Delta Q_{IB,t}^{max}$	Maximum output of IBDR at time t
$\Delta L_{IB,t}^{min}$	Minimum output of IBDR at time t
x_i^k	Position vector of the ith particle in the kth generation
d	Concentration dividing distance
p_l	Fitness of optimal location of low-concentration particle swarm
$f\left(x_i^t\right)i$	Fitness objective function of particle i
$x_{i,k}^t$	Chaotic variable of particle i iteration in the kth dimension of the tth generation
$x_{i,k}^{'t}$	New particle generated by particle i through chaotic search
ω_i^t	Iterative inertial weight of particle i in tth
$u_{CGT,t}$	Start–stop state variable of CGT at time t
$u_{P2G,t}$	Start–stop status variable of P2G at time t
$u_{EC,t}^{in}$	Energy storage of EC at time t
$u_{EC,t}^{out}$	Release status variables of EC at time t
$u_{EC,t}^{ch}$	Status of energy storing at time t
$u_{EC,t}^{dis}$	Status of energy releasing at time t
$u_{GS,t}^{P2G}$	Start–stop status of GS at time t
$g_{MEG,t}$	Power output of MEG at time t
$R_{CGT,t}^{*}$	Revenue after revising the output of CGT at time t
$R_{GB,t}^{*}$	Revenue after revising the output of GB at time t
$P_t^{e,h,c}$	Prices of power, heating and cooling after PBDR at time t

extension, the micro energy grid (MEG) being the power supply system for the internet of energy terminal (Ju et al., 2020).

MGs are power systems located next to the main distribution network (in the island or connected mode) for power storage

using renewable energy sources (RES) and connect to the distribution network when needed for specific purposes. Having high diversity, the MG is a promising technology that enhances consumer reliability and reduces energy costs. MGs have expanded from small prototypes to large-scale commercial ones. MG energy management systems are important factors that play a critical role in the effectiveness and efficiency of MGs (Hannan et al., 2020). The most important advantages of an MG are summarized as follows (Ju et al., 2020; Hannan et al., 2020; Li and Xu, 2019; Lu et al., 2020):

- Controllable power resources and energy storage (ES) systems in an MG can manage and control the generation of renewable sources and, as a result, improve the power quality.
- An MG can provide a variety of services to all loads; for example, it can feed the important loads with reliable power, while it provides cheaper power with lower reliability for less important loads.
- In distribution networks, MGs act as a virtual resource or load. Therefore, the peak load can be corrected through synchronous control of distributed production and loads. Furthermore, the adverse effects of distributed generations can be reduced by MGs, and therefore, help the users of the distribution network because of its easier management.
- Due to their independent operation, MGs help the distribution networks with self-healing mechanisms after the faults.
- An MG can consist of consumers, power companies, or independent third parties. This type of relationship and multifaceted operation encourages all stakeholders to develop and expand renewable energy resources and promote fundamental changes in the market model and energy mechanisms.

In recent years, the developed MEG has been considered by researchers. Some MEGs are based on poly-generation MG (PM). The European knowledge has proposed "Smart Grids" as a power grid which can define the measures of all the linked users - generators, consumers, and those who do both" for efficient, economical, and safe electricity supplement (Jadidbonab et al., 2019). The PM project consists of combined heat and power (CHP) units along with photovoltaic (PV) panels, solar photothermal generators, and different energy storage devices, which can economically provide electrical and thermal energy. Since not all of the renewable sources (wind and solar) are distributable, the suggested energy organization can be used for alternative energy resources. Moreover, the best possible control plan is proposed for both thermal and electrical processes in an MG of several buildings through the CHP, PV panels, electric vehicle, and heat pump (Kumar et al., 2019). Fuel cells and electricity and heat storage devices have been considered in both PM and MEG to allow alternative renewable energy resources.

MEG can convert surplus energy into methane by an electric-to-gas converter and provide cooling, heating, and gas. The power-to-methane conversion is considered as a reverse conversion and cyclic energy. Also, PM focuses on its energy supply which is protected by the superior energy grid. MEG emphasizes active participation in the energy trade by the higher energy grid with respect to the real prices of electricity, cooling, heating, and gasoline.

In particular, the methane produced by the MEG can be sold to an upstream grid or be used for power generation or heating. Therefore, it is a decision-making action for MEG to select the way of achieving optimal energy. In 2016, China National Development suggested some comments on strengthening the smart energy of "Internet +"; this shows it is very essential to strengthen the synchronization of multiple energies. MEG can complement several synchronous energies, and mostly focuses on the synchronous planning of multiple energies from alternative renewable energy resources.

Hence, MEG was studied by researchers around the world from three points of view: system configuration, uncertainty modeling, and operational strategies. The wind turbine, PV, biogas plant, and hydropower plant are integrated into an MEG depending on the system configuration. To optimize equipment capacity and operational strategy, a combined solar, cooling, and heating system is designed. To model the uncertainties, the alternative energy resources should be considered as random variables in the planning model (Bahramara et al., 2019). For operational strategies, previous studies have largely synchronized the optimal performance of various energy devices to provide optimal operating costs and environmental benefits. In Wang et al. (2019), the optimization performance of MEG and combined alternative renewable energy resources was discussed. Moreover, smart grid equipment provided possible conditions for DR to join the power system. As an optimal alternative resource for fossil fuels, new energy sources are very important due to their features, such as sustainability, affordability, and environmental friendliness.

However, as a disadvantage, new energy sources have low reliability due to uncertain and random generation patterns. Combining the energy resources with energy storage systems can reduce the system reliability problem. Therefore, in Moghaddas-Tafreshi et al. (2019), a hybrid grid that is connected to the main grid was proposed which consists of wind and solar as primary energy resources with a hydrogen storage system (fuel cell and electrolyzer) as a backup source. A new power management strategy was presented for accurate load distribution between the MG units. The combined control method (central and distributed) was considered to achieve the control objectives, such as DC-bus voltage regulation, power factor control, synchronous connection to the network, and power oscillation damping. Distributed controllers are responsible for providing local objectives, including maximum power point tracking (MPPT) and storage system control. On the other hand, the central controller is mainly responsible for power management in the MG. In Leonori et al. (2020), MGs consisting of solar cells, micro-turbines, storage devices, and loads were studied. Based on the specific structural analysis of the microgrid and the practical modes of each micro-source, the energy management program was presented and designed. The energy management program and its control strategies were investigated under conditions of network connection and islanding mode. Several algorithmic examples were investigated through simulation and the results confirmed the validity of energy management control strategies.

In recent years, microgrids have emerged as a key component to increase the efficiency, reliability, and stability of electrical infrastructure. The micro-distribution systems are combined modular electrical, local load, and distributed memory renewable power resources that are used for power exchange with the main grid in the connected mode. One of the main tasks in microgrid operation is the dynamic balance of local supply and power demand for the alternative nature of renewable energy resources and load demand change. Nonetheless, the power transmission between the main grid and microgrid is usually dependent on the cost of power loss in the distribution line. In Li et al. (2020), a multi-factor distribution system was required for the optimal synchronization of multiple energy resources. The factors associated with each microgrid were investigated from a participatory strategy to minimize the power loss in the distribution line and to maximize the economic revenue by selling the surplus power generated to other microgrids belonging to a compound. Most of the power management systems are generally based on central

controllers. For example, the centralized energy management system (EMS) is used to manage power converters in the microgrid consisting of wind and PV systems, as described in Ambia et al. (2014). In Elsied et al. (2015), a centralized EMS was used to synchronize the microcontrollers and the main grid was used to minimize greenhouse gas emissions (GHG) and energy costs. It could also maximize the output power of renewable energy systems. Moreover, in Wang et al. (2014), a central microgrid controller was used to optimize supply and demand and reduce fuel costs. The EMS architecture is demonstrated in Fig. 1. The central monitoring controller was employed to optimize the consumption of distributed energy resources (DER) based on fossil fuels, renewable DERs, and energy consumption in the microgrids. This controller generally consists of a communication network that monitors DERs and transmits commands to the local controller to use the power of uncontrollable resources by the most desirable economic method. Regardless of overall success, this method uses a top-down system with problems. Here, there is an error point, which means it is safely composed of appropriate plugin structures. In addition, by increasing the number of generators and loads, we will have higher communication costs for scheduling and online monitoring. Furthermore, after making changes in the microgrid structure or at the time of installing new generators or loads, the central controller is required to be updated. The central control methods can be applied to find the best control strategy. However, a strong computational ability is required, because a large amount of data exist in the system that will lead to further complexity. Moreover, a network with communication potential and a highly distributed control strategy is required (Wang et al., 2017).

In this paper, the MEG problem is considered based on a bidding strategy with the utility network. In Ju et al. (2021), a new multi-level bidding strategy model is presented based on multi-MEGs, which is developed in various steps, i.e., day-ahead/intra-day/real-day in a 3-step solution model. A customer comfort-aware, demand response-integrated long-term microgrid planning optimization model was proposed in Mohseni et al. (2021). The approach (a) uses non-cooperative game theory and Stackelberg leadership principles to recognize and reproduce the planned manners of energy utilities, demand response aggregators, and end-consumers, (b) generates ideal trade-offs among imported power from the main network and accessible demand response resources, and (c) controls the most cost-effective resource placement for energy organization. (4) Delivers a level playing field for evolving equipment, as power-to-gas and vehicle-to-grid involvements (Azeem et al., 2021). The major components and duties of renewable energy resources for the smart city (such as solar, wind, geothermal, hydropower, ocean, and biofuels) were extensively introduced in Hoang and Nguyen (2021). In addition, the technological and economic aspects of integrating renewable energy sources into smart city energy systems were carefully examined.

The articles above about MEG focus on scheme pattern, uncertainty modeling, and operational plans. Nevertheless, there are three most important drawbacks: (i) earlier studies have taken into account the integration of CCHP, PV, WPP, and energy storage, while there are many other energy resources to consider in an MG. (ii) the employed methods have limitations in analyzing the impact of uncertainty of alternative renewable energy resources. On the other hand, earlier studies have only considered DR of energy load, which is accessible for cooling, heating, and gas as well. Another important issue is to use DR to improve the MEG optimization. The 2-stage optimization theory, unlike the aforesaid technique, splits the decision-making process into two stages: pre-decision and real-time decision that corresponds to the MEG optimum scheduling decision process. Third, DR can help with peak shaving and suppressing new energy fluctuations. Another essential problem is utilizing the DR of electricity, heating, cooling, and other energy to enhance MEG operating optimization. In contrast to the above method, the new multi-level optimization approach with the developed artificial bee colony algorithm can achieve the best results with significantly high performance. According to the provided description, the most important innovations of this article are as follows:

1. A new structure for MEG, consisting of various electricity production (EP), energy conversion (EC), and ES devices, is designed considering a different DR from energy. Incentive-based DR (IBDR) and Price-based DR (PBDR) are used to get the optimizing effect of the side-energy bond.
2. A synchronous two-stage planning is presented for an MEG with WPP and PV uncertainties. The upper-layer day-time synchronized energy model considers the results of the day-ahead prediction as random variables in order to maximize the operating revenue. The planning model of lower-layer energy includes a modified ES model and the DR planning model with respect to the real output.
3. An improved artificial bee colony optimization algorithm is proposed, and its local and global search is significantly improved. Next, with respect to different scenarios of model investigation, the outcome of PBDR and power-to-gas (P2G) optimization on MEG performance is discussed.

2. The overall view of the MEG

MEG is an integrated micro-energy connection system that supplies energy requirements using local RES. It is composed of various sections such as EC, EP, and ES systems. EP consists of some sections such as solar, wind, gas boilers (GB), and conventional gas turbines (CGT). EC consists of electricity to gas, power to cooling, energy to heating, and heating to cooling. ES consists of cooling, heating, electricity, and gasoline storages. DR can utilize the time-of-use (TOU) price to guide the consumers to regulate their energy consumption pattern considering load profile. As a result, DRs of multiple loads have been measured. In addition, the valley period refers to the period with a low demand load. For electricity load, mostly at night, P2G and GST can convert energy into natural gas, which then can be converted to electrical power or heating. To achieve cascade conversion, the multi-directional energy can be converted into cooling by P2C and H2C. The overview of MEG is shown in Fig. 2.

3. MEG problem modeling

3.1. EP model

(A) WPP output model

WPP output power depends on rate of speed of wind. When the wind speed is less than its minimum value, it makes WPP generate power. Also, when the wind speed exceeds the maximum level, the wind turbine is locked for safety. The power generated by the wind energy is calculated as follows:

$$g^*_{WPP,t} = \begin{cases} 0, & 0 \le v_t \le v_{in}, v_t > v_{out} \\ \dfrac{v_t - v_{in}}{v_{in} - v_{rated}} g_R, & v_{in} \le v_t \le v_{rated} \\ g_R, & v_{rated} \le v_t \le v_{out} \end{cases} \quad (1)$$

(B) PV output model

PV power generation is mostly related to the intensity of solar radiation and the area of PV panels. The power generated by the PV system can be calculated as follows:

$$g^*_{PV,t} = \eta_{PV} \times S_{PV} \times \theta_t \quad (2)$$

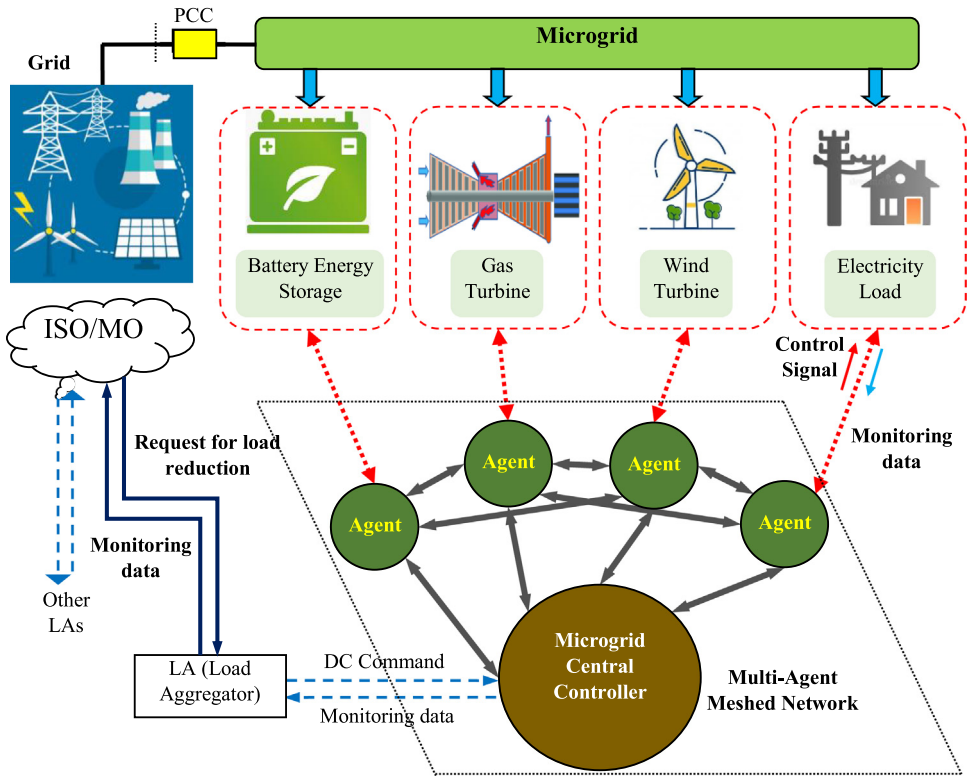

Fig. 1. General concept of a microgrid.

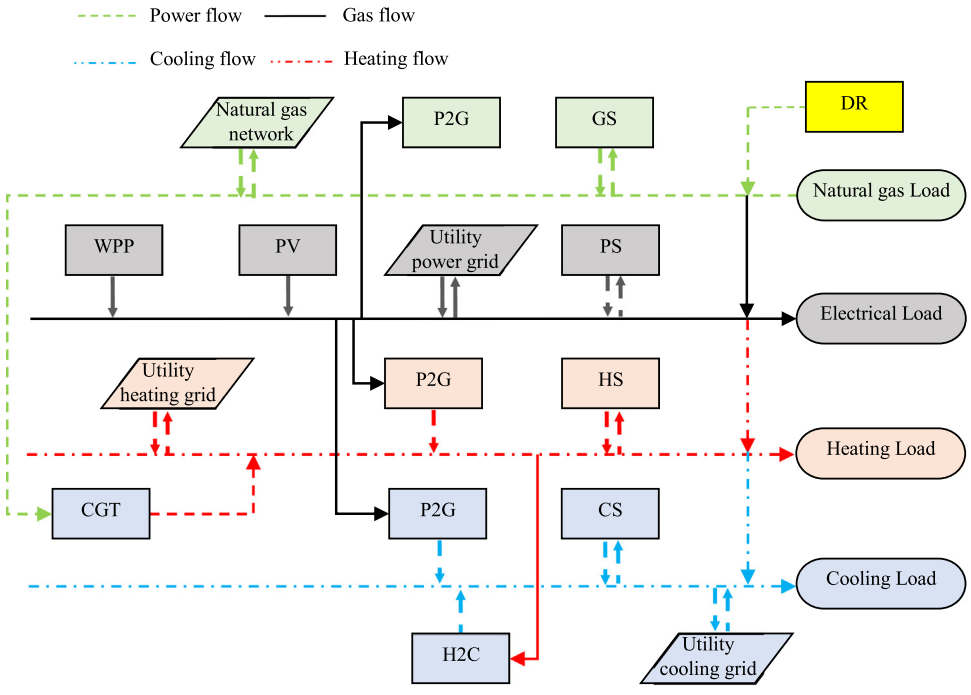

Fig. 2. Basic structure for microgrids based on power, heating, and cooling flow.

(C) CGT output model can provide the heating system through the heating system.

$$g_{CGT,t} = V_{CGT,t} H_{ng} \eta_{CGT,t} \tag{3}$$

$$\mathcal{Q}_{CGT,t} = V_{CGT,t}(1 - \eta_{CGT,t} - \eta_{loss})\eta_{hr} \tag{4}$$

(D) GIGABYTE output as supplementary heating is provided by GB.

$$\mathcal{Q}_{GB,t} = V_{GB,t} H_{ng} \eta_{GB} \tag{5}$$

3.2. EC model

(A) P2G device

P2G uses the limited output of PV and WPP to convert CO_2 to CH_4, which leads to the connection of the electricity network and the gas network. The exact performance model can be mathematically expressed by:

$$V_{P2G,t} = g_{P2G,t}\varphi_{P@G}/H_{ng} \tag{6}$$

In addition, the ratio of natural gas supplied using P2G and inserted into CGT, GB, GST, and natural gas networks is $\eta_{P2G,t}^{CGT}$, $\eta_{P2G,t}^{GB}$, $\eta_{P2G,t}^{GST}$, $\eta_{P2G,t}^{NG}$. According to Eqs. (3) – (5), the power and heat increase in CGT generation are Δg_{CGT}^{P2G} and Δg_{CGT}^{P2G}, respectively. The increased GB heating is $\Delta Q_{GB,t}^{P2G}$.

(B) Additional EC equipment

EC also consists of P2H, P2C, and H2C that can be modeled by:

$$\begin{bmatrix} Q_{P2C,t} \\ Q_{P2H,t} \\ Q_{H2C,t} \end{bmatrix} = \begin{bmatrix} g_{P2C,t} & 0 & 0 \\ 0 & g_{P2H,t} & 0 \\ 0 & 0 & Q_{H2C} \end{bmatrix} \begin{bmatrix} \varphi_{P2C} \\ \varphi_{P2H} \\ \varphi_{H2C} \end{bmatrix} \tag{7}$$

3.3. ES model

(A) GS system can store excess natural gas starting P2G with respect to the price of gasoline, power, and heating:

$$V_{GS,t}^{P2G} = V_{P2G,t}\left(\eta_{P2G,t}^{GS} - \eta_{P2G,t}^{loss}\right) \tag{8}$$

$$S_{GS,t} = S_{GS,T_0} + \sum_{t=1}^{T}\left(V_{GS,t}^{P2G} - V_{GS,t}^{CGT} - V_{GS,t}^{GB} - V_{GS,t}^{NG}\right). \tag{9}$$

(B) Additional ES equipment

ES also consists of HS, PS, and CS. ES can store energy in the valley-load periods and discharge energy in the peak times.

$$Q_{ES,t} = u_{ES,t}^{ch} Q_{ES,t}^{ch} - u_{ES,t}^{dis} Q_{ES,t}^{dis} \tag{10}$$

$$S_{ES,t} = \left(1 - \eta_{ES,t}^{loss}\right) S_{ES,t-1} + \left[Q_{ES,t}^{ch}\varphi_{ES,t}^{ch} - Q_{ES,t}^{dis}/\varphi_{ES,t}^{dis}\right] \tag{11}$$

4. Two-stage synchronized planning plan

4.1. Stochastic model

It consists of two aspects, which means the difference between the predicted value of the day before and the real value, and oscillation over time. Based on Weibull distribution functions, we have (Usta et al., 2018):

$$f(v) = \frac{\varphi}{\vartheta}\left(\frac{v}{\vartheta}\right)^{\varphi-1} e^{-(v/c)^{\varphi}} \tag{12}$$

$$f(\theta) = \begin{cases} \dfrac{\Gamma(\omega)\Gamma(\psi)}{\Gamma(\omega)+\Gamma(\psi)}\theta^{\omega-1}(1-0)^{\psi-1}, & 0 \le \theta \le 1, \\ & \omega \ge 0, \psi \ge 0 \\ 0, & otherwise \end{cases} \tag{13}$$

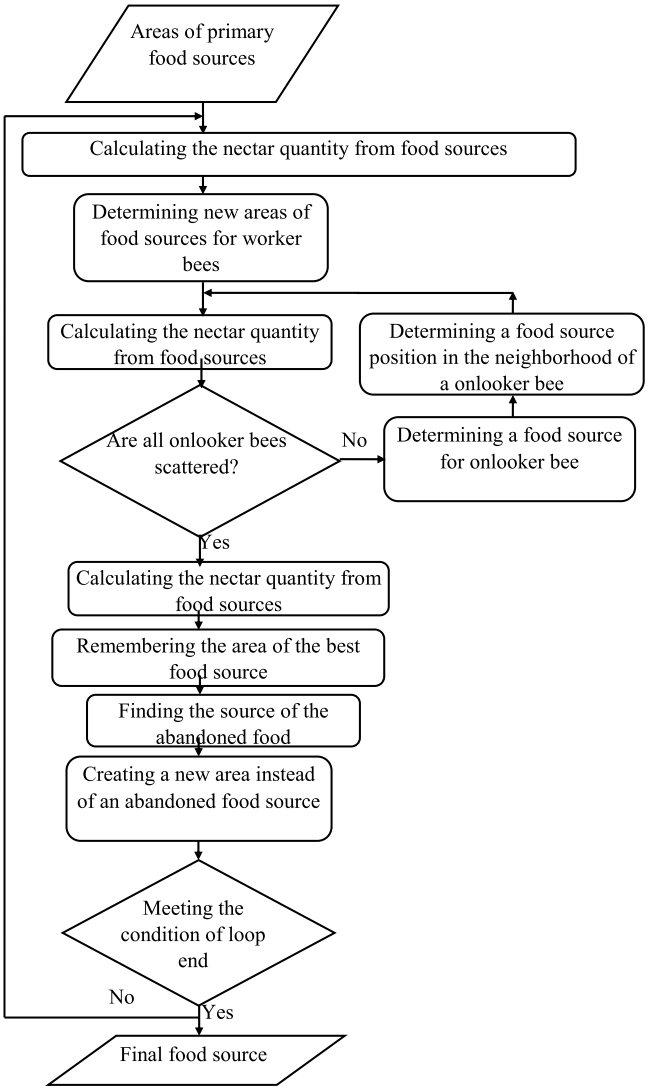

Fig. 3. Flowchart of the ABC algorithm.

where v is the wind speed, parameters φ and ϑ are mode and scale, θ represents solar radiation, ω and ψ are mode parameters. In the suggested scheme, the time horizons of the day-ahead and the real-time model are 24 h, but the input data in the lower and upper layers are dissimilar. The suggested two-step scheme is mostly employed to resolve the uncertainty of RES, especially PV and WPP.

During the upper-layer day-time synchronized plan, the outputs of RES are regarded as random variables. Based on the predicted data of the forecasted day, the start–stop status of all devices is determined, which allows for operational limits of the various energy and storage equipment of the system.

During the lower-layer real-time planning plan, the real outputs of RES are regarded as the random variables, and deviation of WPP and PV output is investigated using developing the ES performance. If deviation cannot be corrected, it is called IBDR, which balances the demand for power, heating, and cooling load.

4.2. Upper-layer synchronized model

Based on the forecasted results of the uncertainty variables, the upper-layer model performs an operational planning program

Input: X_i

Output: X_i^{new}

Start

Step1. Set k=1 (current iteration) and k_{max}=200 (maximum number of iterations).

Step 2. Initialize chaotic variables $y_{k,j} \in [0,1]$ randomly, $\forall j \in \{1,2,...,D\}$.

Step 3. Compute intermediate chaotic variable using $y_{k+1,j} = \mu y_{k,j}(x_j^{\max} - x_j^{\min}), \forall j \in \{1,2,...,D\}$

Step 4. Compute target solution using $x_{ij}^{new} = x_j^{\min} + y_{ij}(x_j^{\max} - x_j^{\min})$

Step 5. If $f(x_i^{new}) < f(x_i^{new})$ then

Substitute solution with candidate solution x_i^{new}, Set $trials(i) = 0$ and exit

Else

Set $trials(i) = trials(i) + 1$, $k = k + 1$ go to Step 3.

End

Finish

Fig. 4. Model Developed for chaos theory to be used in artificial bee colony algorithm.

and determines the start–stop status of the various units. Maximum operating revenue is considered as the goal of optimization.

$$MaxR_{upper} = \sum_{j=1}^{\tilde{N}} q_j \times \sum_{t=1}^{T} \left[\underbrace{\begin{pmatrix} R_{WPP,t} + R_{PV,t} + \\ R_{CGT,t} + R_{GB,t} \end{pmatrix}_j}_{R_{EP,t}} + \underbrace{\begin{pmatrix} R_{P2G,t} + R_{P2H,t} + \\ R_{P2C,t} + P_{H2C,t} \end{pmatrix}_j}_{R_{EC,t}} + \underbrace{\begin{pmatrix} R_{PS,t} + R_{GS,t} + \\ R_{HS,t} + R_{CS,t} \end{pmatrix}_j}_{R_{ES,t}} \right] \tag{14}$$

For PV and WPP, the cost margin of electricity production is basically zero. The operating revenue is calculated based on the price and quantity. In the CGT, the operating revenue is equal to the electricity and heating revenue subtracted by energy costs, which is formulated as follows:

$$\begin{aligned} R_{CGT,t} = & \left\{ P_{CGT,t}^{e} g_{CGT,t} + P_{CGT,t}^{h} Q_{CGT,t}^{h} \right\} \\ & - \left\{ P_{ng,t} \left[a_i \left(g_{CGT,t} + \theta_h Q_{CGT,t}^{h} \right)^2 \right. \right. \\ & \left. \left. + b_i \left(g_{CGT,t} + \theta_h Q_{CGT,t}^{h} \right) + c_i \right] \right\} \\ & - \left\{ \left[\mu_{CGT,t}^{up} \left(1 - \mu_{CGT,t-1}^{up} \right) \right] C_{CGT,t}^{up} \right. \\ & \left. + \left[\mu_{CGT,s}^{dn} \left(1 - \mu_{CGT,s+1}^{dn} \right) \right] C_{CGT,s+1}^{dn} \right\} \end{aligned} \tag{15}$$

The revenue of this operation is equal to the revenue of energy supply subtracted by energy consumption cost, which is formulated as follows:

$$R_{EC,t} = P_{EC,t}^{out} E_{EC,t}^{out} \varphi_{EC,t}^{out} - P_{EC,t}^{in} E_{EC,t}^{in} / \varphi_{EC,t}^{in} \tag{16}$$

For ES, as shown in the following equation, the operating revenue is equal to the revenue obtained from the energy storage costs:

$$R_{ES,t} = P_{ES,t}^{dis} Q_{ES,t}^{dis} \varphi_{ES,t}^{dis} - P_{ES,t}^{ch} Q_{ES,t}^{ch} / \varphi_{ES,t}^{dis} \tag{17}$$

To ensure optimal MEG performance, energy supply limits, and demand equilibrium, the performance of EC, EP, and ES devices must be measured.

(1) Energy supply and balance

$$\begin{aligned} & \left(g_{CGT,t} + \Delta g_{CGT,t}^{P2G} + \Delta g_{CGT,t}^{GS} \right) (1 - \varphi_{CGT}) - Q_{PS,t}^{dis} \\ & + g_{UG,t} = Q_t^{e} - g_{RE,t} + g_{P2C,t} + g_{P2H,t} + g_{P2G,t} + Q_{PS,t}^{ch} + \Delta Q_t^{PB,e} \end{aligned} \tag{18}$$

$$\begin{aligned} & Q_{CGT,t} (1 - \varphi_{CGT}) + Q_{GB,t} (1 - \varphi_{GB}) + \Delta Q_{GB,t}^{GS} \\ & + \Delta Q_{GB,t}^{P2G} + \Delta Q_{CGT,t}^{P2g} + \Delta Q_{CGT,t}^{GS} + Q_{P2H,t} - Q_{HS,t}^{dis} \\ & = Q_t^{h} + Q_{H2C,t} + Q_{HS,t}^{ch} + \Delta Q_t^{PB,h} \end{aligned} \tag{19}$$

$$Q_{H2C,t} + Q_{P2C,t} - Q_{CS,t}^{dis} = Q_t^{c} + Q_{CS,t}^{ch} + \Delta Q_t^{PB,c} \tag{20}$$

Based on the principles of microeconomics, the PBDR can be expressed by:

$$E_{st} = \frac{\Delta Q_s / Q_s^0}{\Delta P_t / P_t^0} \begin{cases} E_{st} \le 0, s = t \\ E_{st} \ge 0, s \ne t. \end{cases} \tag{21}$$

Changes in power load, heating, and cooling after PBDR can be calculated as follow:

$$\begin{aligned} \Delta Q_t^{PB,(e,h,c)} = Q_t^{e,h,c} \times \left\{ E_{tt}^{e,h,c} \times \frac{\left[P_t^{e,h,c} - P_t^{(e,h,c),0} \right]}{P_t^{(e,h,c),0}} + \sum_{\substack{s=1 \\ s \ne t}}^{24} E_{st}^{e,h,c} \right. \\ \left. \times \frac{\left[P_s^{e,h,c} - P_s^{(e,h,c),0} \right]}{P_s^{(e,h,c),0}} \right\} \end{aligned} \tag{22}$$

(2) EP performance limits

CGT regulates the output by adjusting the generated condensed steam. On the other hand, the larger the extraction capacity, the smaller the steam ratio used for regulation. These limits are mathematically expressed as follows:

$$\begin{aligned} & max \left\{ g_{CGT}^{min} - c_{min} Q_{CGT}, c_m \left(Q_{CGT} - Q_{CGT}^{0} \right) \right\} \le g_{CGT} \\ & \le g_{CGT}^{max} - c_{max} Q_{CGT} \end{aligned} \tag{23}$$

$$0 \le Q_{CGT} \le Q_{CGT}^{max} \tag{24}$$

$$\begin{aligned} & u_{CGT,t} \left(g_{CGT}^{min} + \theta_h Q_{CGT,t}^{min} \right) \le g_{CGT,t} + \theta_h Q_{CGT,t} \\ & \le u_{CGT,t} \left(g_{CGT,t}^{max} + \theta_h Q_{CGT,t}^{max} \right) \end{aligned} \tag{25}$$

(2) EC performance limits

EC should satisfy the minimum and maximum energy limits.

$$u_{P2G,t} V_{P2G,t}^{min} \le V_{P2G,t} \le u_{P2G,t} V_{P2G,t}^{max} \tag{26}$$

$$u_{EC,t}^{out} E_{EC,t}^{out,min} \le E_{EC,t}^{out} \le u_{EC,t}^{out} E_{EC,t}^{out,max} \tag{27}$$

$$u_{EC,tEC,t}^{in} E_{EC,t}^{in,min} \le E_{EC,t}^{in} \le u_{EC,t}^{in} E_{EC,t}^{in,max} \tag{28}$$

$$u_{EC,t}^{in} + u_{EC,t}^{out} \le 1 \tag{29}$$

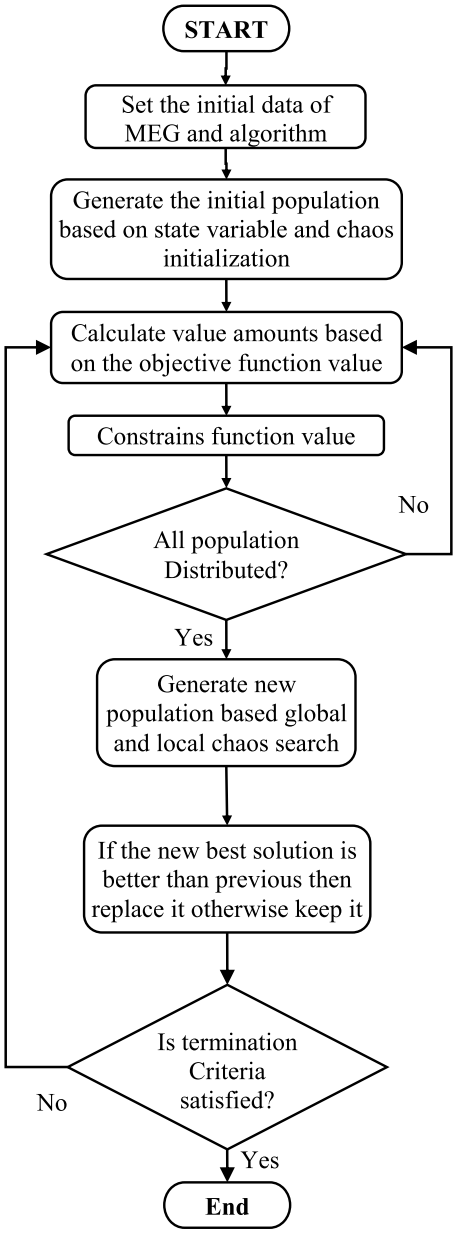

Fig. 5. Flowchart of proposed solution model in Energy management problem in MEG.

(3) ES performance limits

ES must satisfy the minimum and maximum energy storage limits.

$$u^{ch}_{ES,t}Q^{ch,min}_{ES,t} \le Q^{ch}_{ES,t} \le u^{ch}_{ES,t}Q^{ch,max}_{ES,t} \tag{30}$$

$$u^{dis}_{ES,t}Q^{dis,min}_{ES,t} \le Q^{dis}_{ES,t} \le u^{dis}_{ES,t}Q^{dis,max}_{ES,t} \tag{31}$$

$$S^{min}_{ES,t} \le S_{ES,t} \le S^{max}_{ES,t} \tag{32}$$

$$u^{P2G}_{GS,t}V^{P2G,min}_{GS,t} \le V^{P2G}_{GS,t} \le u^{P2G}_{GS,t}V^{P2G,max}_{GS,t} \tag{33}$$

$$S_{ES,T_0} = S_{ES,T}. \tag{34}$$

(4) The reserve system for MEG must have sufficient capacity. Thus, to deal with WPP and PV uncertainties, a certain capacity for power is predetermined.

$$g^{max}_{MEG,t} - g_{MEG,t} + Q^{dis}_{PS,t} \ge r^e Q^e_t + r_{WPP}g_{WPP,t} + r_{PV}g_{PV,t} \tag{35}$$

$$g_{MEG,t} - g^{min}_{MEG,t} + Q^{ch}_{PS,t} \ge r_{WPP}g_{WPP,t} + r_{PV}g_{PV,t} \tag{36}$$

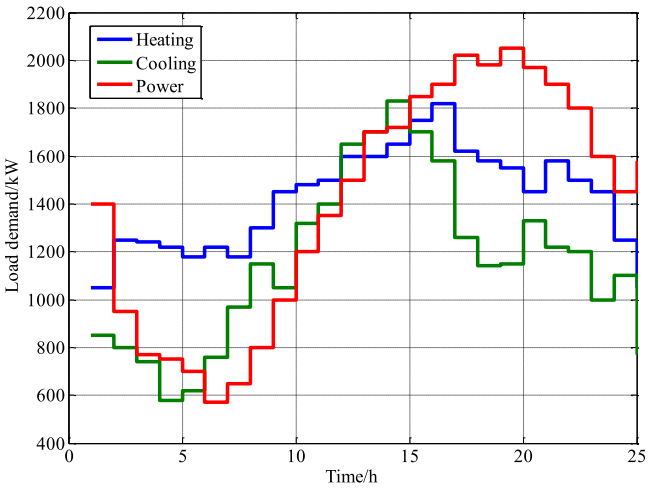

Fig. 6. Demand for heating, power, and cooling on a normal day.

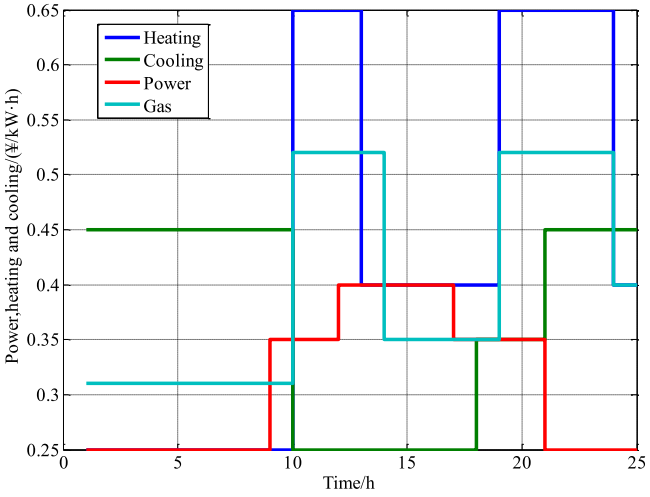

Fig. 7. Price of electricity, cooling, heating, and gasoline in various periods.

MEG must also meet the reserve system's limits and rotational cooling, as in Eq.

4.3. Lower-layer planning model

Since energy planning is a real-time decision-making process, it is essential to deal with the deviation of RES and load between the real and predicted values. Therefore, the above ambiguities are solved in the lower-layer model.

$$minF^{ES}_{lower} = \sum_{j=1}^{\tilde{N}} q_j \sum_{t=1}^{T} \left\{ \left| -\left[\left(g^{dis}_{ES,t} - g^{chr}_{ES,t}\right) + g_{PV,t} + g_{WPP,t}\right] + \left[\left(g^{dis}_{ES,t} - g^{chr}_{ES,t}\right)^* + g^*_{PV,t} + g^*_{WPP,t}\right] \right|_j \right\} \tag{37}$$

shows the real RES outputs at time t, representing the modified ES efficiency at time t, and does not affect the output programs after time t.

After ES activates in the energy release condition:

$$Q_{ES,t'+1} = Q_{ES,t'} - g^{dis}_{ES,t'}\left(1 + \rho^{dis}_{ES,t'}\right) \tag{38}$$

After ES activates in the energy release condition:

$$Q_{ES,t'+1} = Q_{ES,t'} + g^{chr}_{ES,t'}\left(1 - \rho^{chr}_{ES,t'}\right) \tag{39}$$

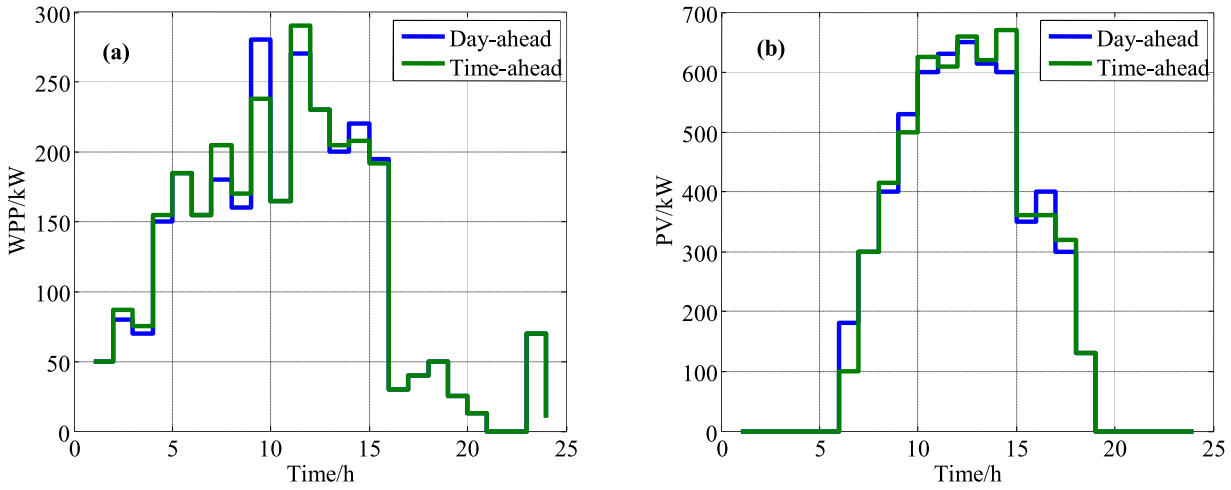

Fig. 8. Output power in the day before and real-time stages, (a) PV and (b) WPP.

When ES cannot be revised, IBDR can provide virtual output.

$$minF_{lower}^{IB} = \sum_{j=1}^{\tilde{N}} q_j \sum_{t=1}^{T} \left[\pi_t^{IB,(e,h,c)} + \left(R_{CGT,t} - R_{CGT,t}^{*}\right) + \left(R_{GB,t} - R_{GB,t}^{*}\right) + P_{GC,}^{e,h,c} Q_{GC,t}^{e,h,c} + P_{SP,t}^{e,h,c} Q_{SP,t}^{e,h,c} \right]_j \quad (40)$$

The temporary efficiency of CGT and GB is a peak-correction service that requires higher prices. $\pi_t^{IB,(e,h,c)}$ denotes the planning cost, cooling, and heating (IBDR) at time t.

$$\Delta Q_{IB,t}^{E} + \Delta Q_{IB,t}^{up} \le \Delta Q_{IB,t}^{max} \quad (41)$$

$$\Delta Q_{IB,t}^{E} + \Delta Q_{IB,t}^{dn} \ge \Delta Q_{IB,t}^{min} \quad (42)$$

After IBDR is implemented to deal with the deviation from load due to uncertainty, the peak capacity of GB and CGT modification can be used to make certain load supply.

$$\left(g_{CGT,t}^{*} + \Delta g_{CGT,t}^{P2G,*} + \Delta g_{CGT,t}^{GS,*}\right)(1-\varphi_{CGT}) - Q_{PS,t}^{dis} + g_{UG,t} = \begin{bmatrix} Q_t^{e} - g_{RE,t} + g_{P2C,t} + g_{P2H,t} + g_{P2\ g,t} + Q_{PS,t}^{ch} + \\ \Delta Q_t^{PB,e} + \Delta Q_t^{IB,e} \end{bmatrix} \quad (43)$$

$$\begin{bmatrix} Q_{CGT,t}^{*}(1-\varphi_{CGT}) + Q_{GB,t}^{*}(1-\varphi_{GB}) + \Delta Q_{GH,t}^{GS,*} + \\ \Delta Q_{GB,t}^{P2G,*} + \Delta Q_{CGT,t}^{P2g} + \Delta Q_{CGT,t}^{GS,*} + Q_{P2H,t} - Q_{HS,t}^{dis} \end{bmatrix} = \begin{pmatrix} Q_t^{h} + Q_{H2C,t} + Q_{HS,t}^{ch} + \\ \Delta Q_t^{PB,h} + \Delta Q_t^{IB,h} \end{pmatrix} \quad (44)$$

$$Q_{H2C,t} + Q_{P2C,t} - Q_{CS,t}^{dis} = Q_t^{c} + Q_{CS,t}^{ch} + \Delta Q_t^{PB,c} + \Delta Q_t^{IB,c} \quad (45)$$

Therefore, the storage capacity must be predetermined:

$$g_{MEG,t}^{max} - g_{MEG,t} + Q_{PS,t}^{dis} + \Delta Q_{IB,t}^{up,e} \ge r^{e} Q_t^{e} + r_{WPP} g_{WPP,t} + r_{PV} g_{PV,t} \quad (46)$$

$$g_{MEG,t} - g_{MEG,t}^{min} + Q_{PS,t}^{ch} + \Delta Q_{IB,t}^{dn,e} \ge r_{WPP} g_{WPP,t} + r_{PV} g_{PV,t} \quad (47)$$

Likewise, the reserved limits and reserved heating must be regulated. While the time horizon of energy organization is calculated per minute, the predetermined storage capacity should be billed.

5. Developed artificial bee colony algorithm

The artificial bee colony (ABC) algorithm reported in the articles is inspired by the behavior of bees in nature. Similar to a natural bee colony, this algorithm also consists of three groups, namely worker, onlooker, and scout bees (Sun et al., 2020).

In this algorithm, first, a set of food sources is randomly selected. The worker bees move to the source and calculate their nectar levels. Next, these bees return to the hive and share their information with other bees (onlookers). Second, after the information exchange, each worker bee goes to the food sources that have already been found and may select a new source in the neighborhood of the previous present one based on visual information received from the environment. This means that a bee decides to go to the present source or select a new source. Third, onlookers choose a range of food sources based on their nectar with respect to the information received from the worker bees in the dance area. After reaching the area, they may select a new source nearby based on visual information. When a source is depleted or abandoned, it is replaced by a new source that is randomly found by the scout bees. This cycle will be repeated until the needs are met. In this model, there is a maximum of one scout bee per cycle and the numbers of worker and onlooker bees are equal.

As mentioned, each of the worker and onlooker bees might make changes to the position of the food source (response) in their memory and calculate its fitness. If its fitness is higher than the old one, the new response is selected and the old one is forgotten. Otherwise, the old response will be left. This selection process is called greedy selection. These changes are obtained by the following equation (Sun et al., 2020):

$$v_{ij} = x_{ij} + \phi_{ij}(x_{ij} - x_{kj}) \quad (48)$$

$$i \ne k,\ \ k \in \{1, 2, \ldots \mathrm{Ne}\},\ j \in \{1, 2, \ldots D\},\ \ \phi_{ij} \in [-11] \quad (49)$$

where ϕ_{ij} is a random number in the range of [−1 1]. This production variable controls the position of neighboring food sources around x_{ij}. In this regard, N_e is the number of worker bees, and the variable k is generated randomly and will be different from i. According to the equation above, as the difference between x_{ij} and x_{kj} decreases, the deviation from x_{ij} will also decrease. In fact, in this equation, we try to select one of the dimensions of one of the positions and, considering the value of ϕ, we move toward it or in the opposite direction. Similar to particle swarm optimization algorithm, the difference is that with random selection, we try to create some variety and prevent the being trapped in a local optimum. After completing the search process, onlookers evaluate the information of each worker bee and select one of the food sources with a probability that is proportional to the quality of the source's nectar. This probability is obtained from the following equation (Sun et al., 2020):

$$p_i = \frac{fit_i}{\sum_{n=1}^{N_e} fit_n} \quad (50)$$

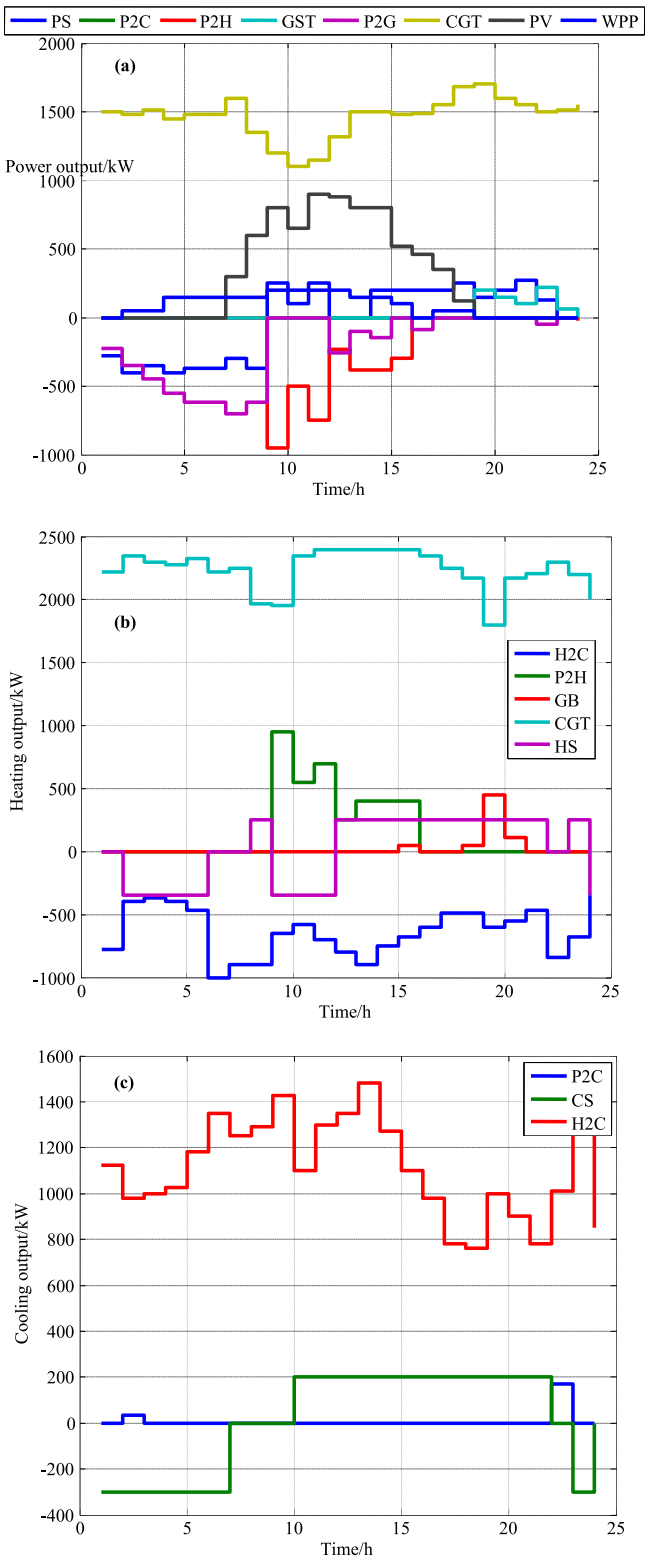

Fig. 9. Optimization results for the upper-layer synchronized model.

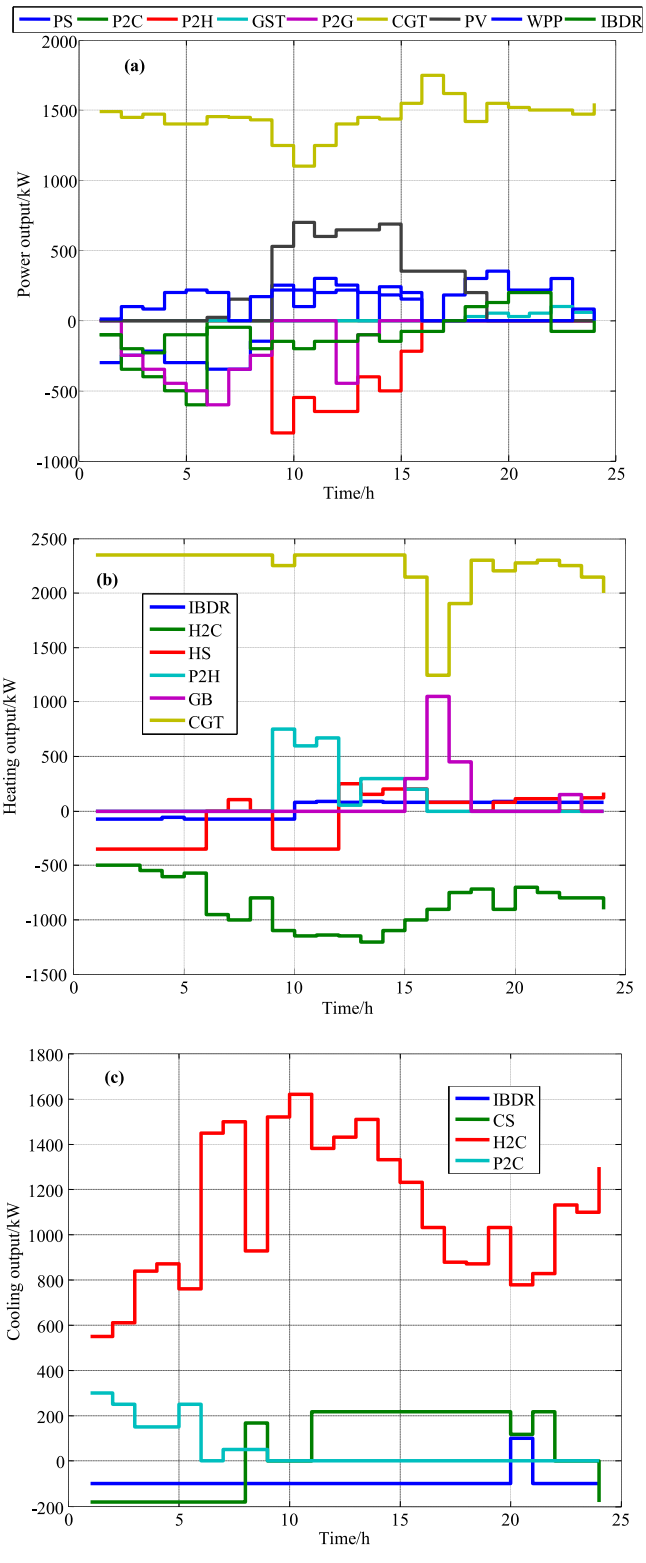

Fig. 10. The optimized results of the lower layer.

where fit $_i$ is the fitness of food source corresponding to the *i*th bee and N_e is the number of available solutions (number of worker bees). If a source runs out or the quality of a food source is not suitable, the worker bee leaves it and turns into a scout. This behavior is modeled such that if the fitness of a point is not improved after several iterations (the number of which is represented by the limit parameter), it is concluded that the optimization is trapped in a local optimum. Therefore, the point is deleted and a new point is generated randomly. The schematic of the ABC algorithm is shown in Fig. 3.

In order to increase the search ability and convergence performance of the algorithm, an independent search for the scout bee

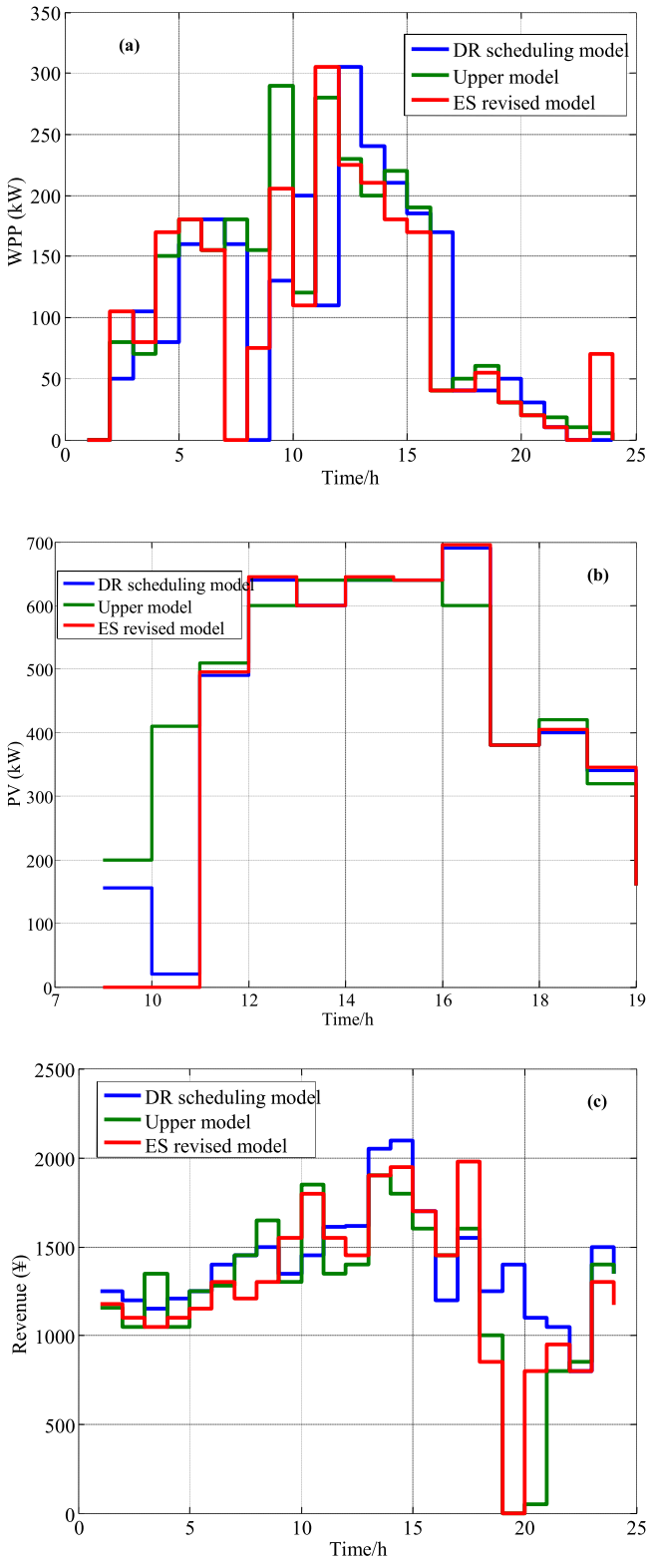

Fig. 11. Planning results of MEG with different models.

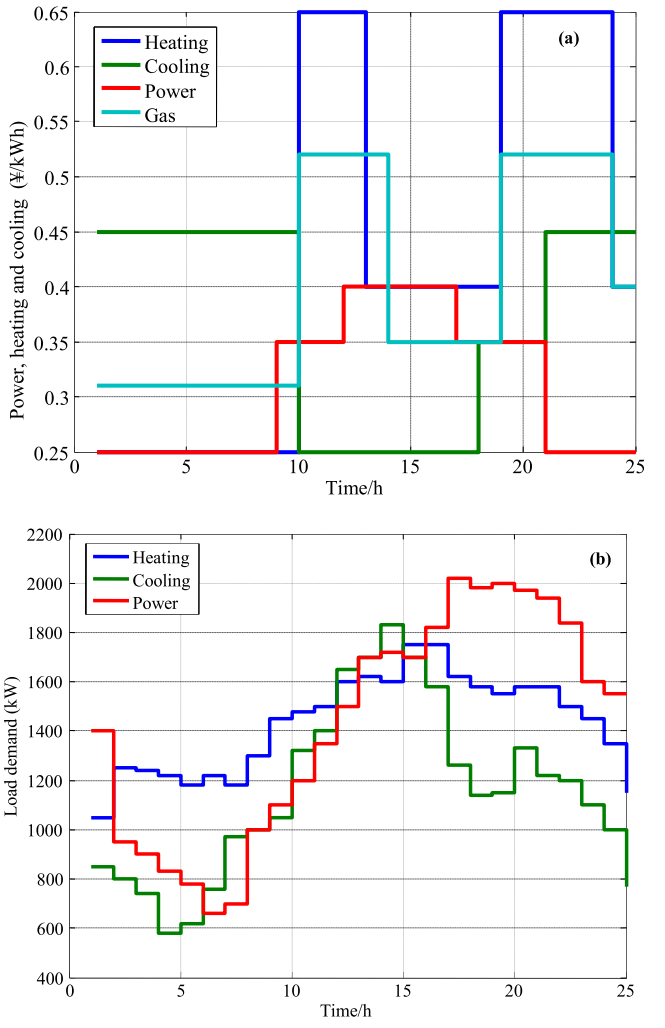

Fig. 12. Demand load and energy price in different periods after implementation of PBDR.

phase is considered. This modification can increase the speed of convergence and follows the following process:

(A) Independent search process: This part is similar to the scout bee. Each scout bee randomly selects a worker bee and follows the equations below. The best solution is returned between the previous and current solutions, and the weakest is determined based on the fitness function and greedy selection strategy:

$$\begin{aligned}
&for \quad \mathrm{i} = 1 : \mathrm{N}_{ont} \\
&\overline{X}_{i,j}(t) = X_{i,j}(t) + \psi_{i,j}(t)(X_{i,j}(t) - X_{k,j}(t)) \\
&X_{i,j}(t) = \begin{cases} \overline{X}_{i,j}(t), & if \ \mathrm{g}(\overline{X}_i(t)) > \mathrm{g}(X_i(t)) \\ X_{i,j}(t), & \text{otherwise} \end{cases} \\
&If \ the \ old \ solution \ is \ updated, \ then \ T_{ri} = 0 \\
&else \ T_{ri} = T_{ri} + 1 \\
&end
\end{aligned} \tag{51}$$

where $\psi_{i,j}(t)$ is a random value between -1 and 1; and $X_{k,j}(t)$ jth is after $\mathrm{X_k}$ solution that is obtained randomly from the search space. N_{ont} represents the number of scout bees that are generally identical to onlooker bees.

(B) Chaos theory: To prevent being caught in a local optimum and improve the exploration of the proposed method, the chaos-based search is also suggested. In this step, when a particle is not improved after the predetermined experiments, it is more likely

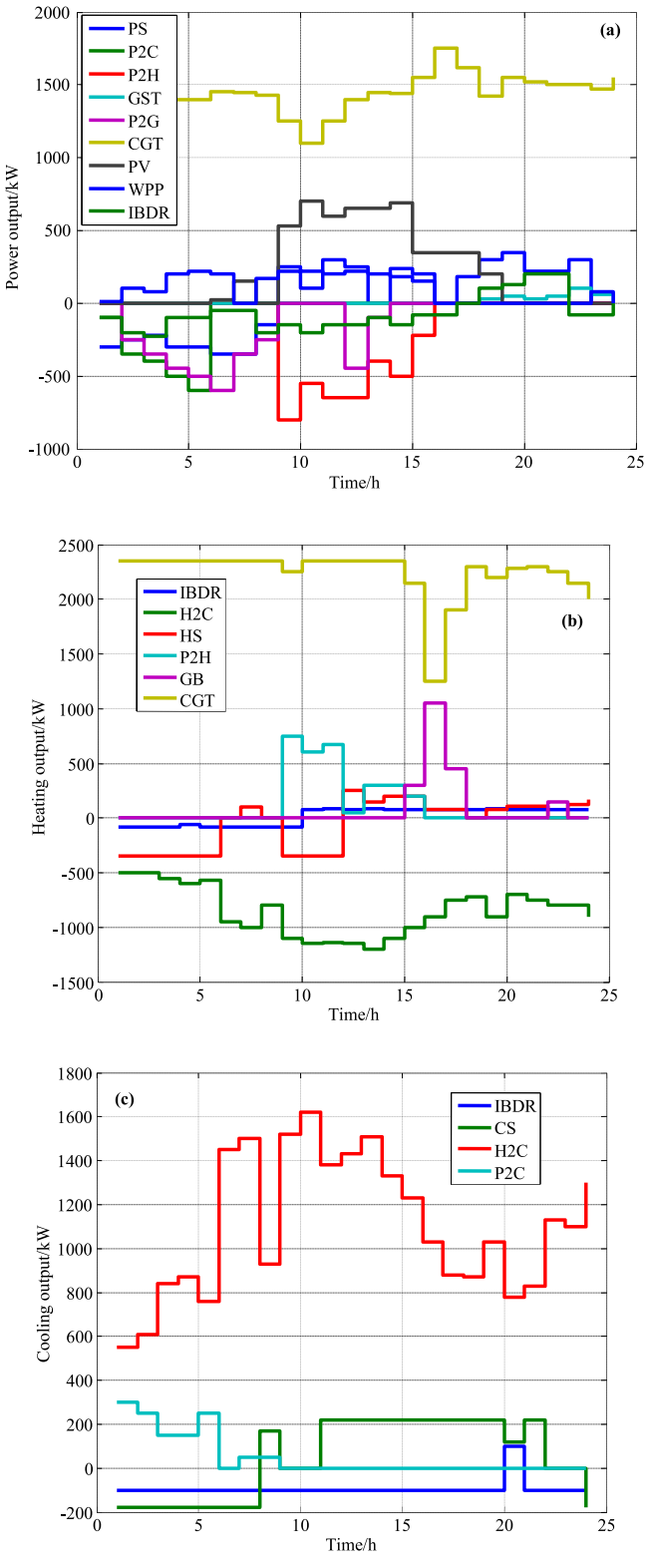

Fig. 13. MEG planning results after PBDR.

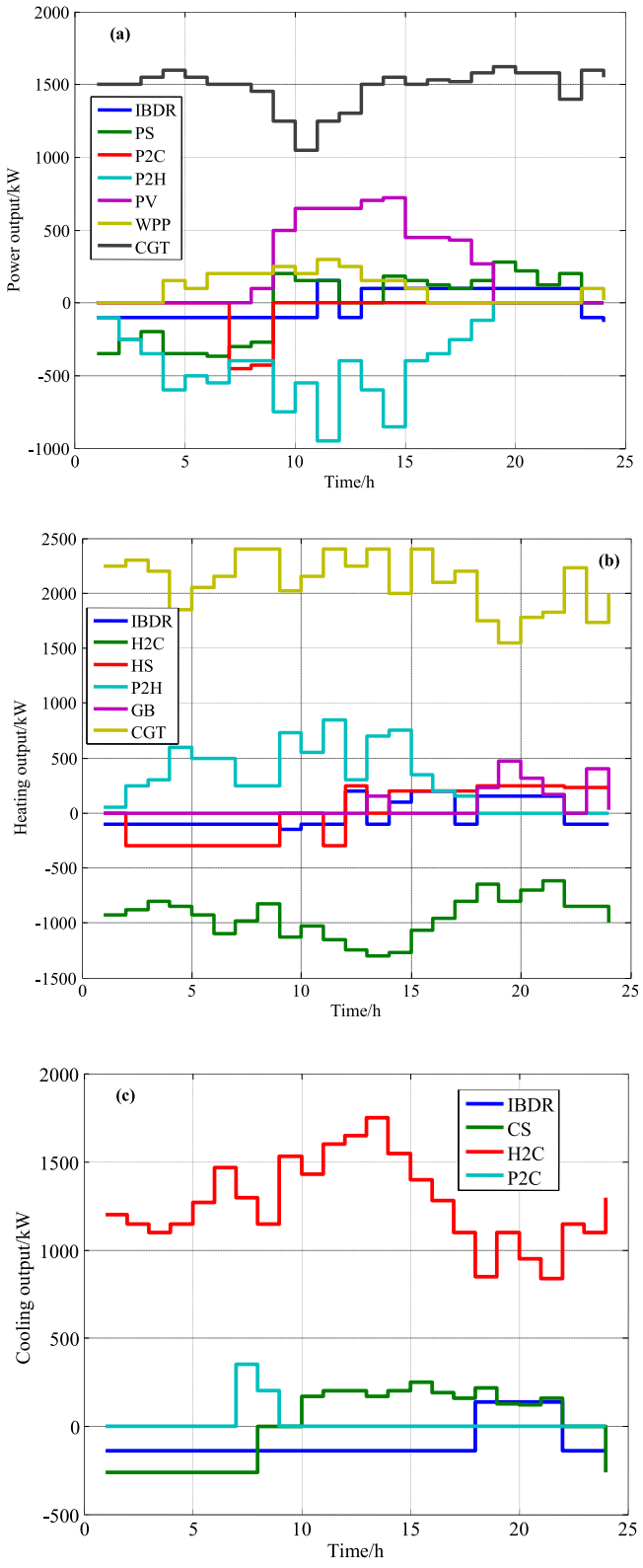

Fig. 14. MEG planning results without P2G.

to get caught in a local optimum and, therefore, be replaced with a new response. Therefore, to prevent premature convergence and improve the algorithm's exploration capability, a chaos-based search method is used. The pseudo-code of this procedure is shown in Fig. 4.

The proposed solution model's flowchart is presented in Fig. 5.

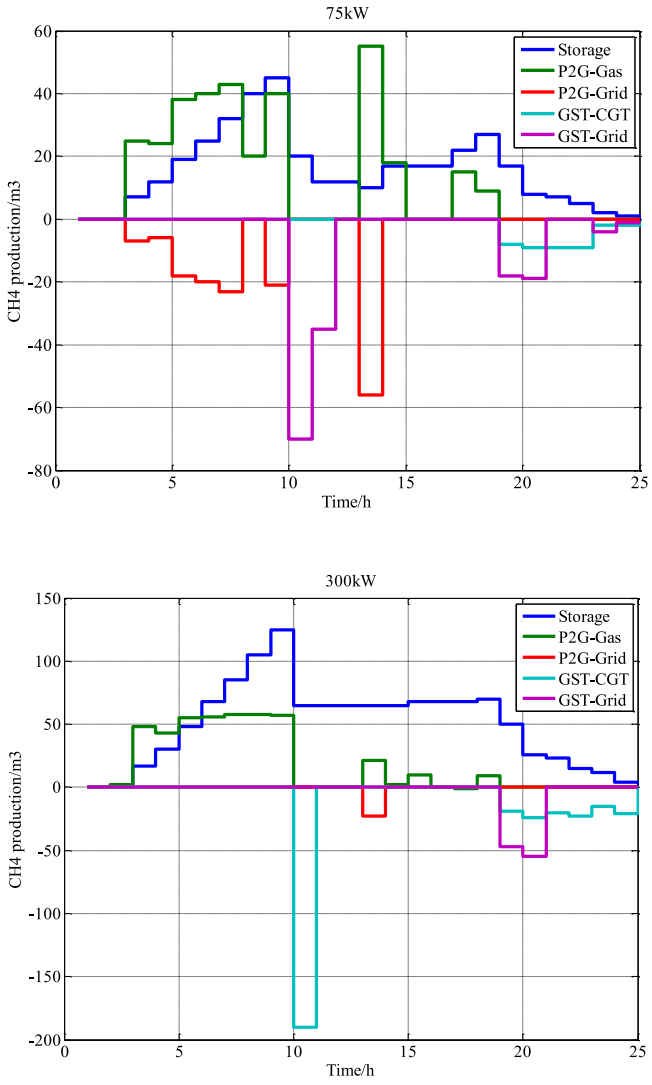

Fig. 15. P2G-GST optimization results with different capacities.

6. Simulation results

6.1. Data of the studied system

Based on the energy planning form and resolution scheme, the simulation is performed by MATLAB software version 2011 Ra. The low carbon park in Longgang, China is selected, to analyze the application of the suggested model. The data of this system can be obtained from Ju et al. (2016) and Ma et al. (2017). Accordingly, the cost performance of CGT is separated into two parts with rise coefficients kW/0.5 ¥ and 15/0 kWW. Next, the GS is installed with a capacity of 500 m^3. The max power of P2G is 150 kW. Table 1 shows the data of the installed energy component in low carbon park.

To make the analysis possible, the performance efficiencies of EP, EC, and ES are considered 96%. The normal daily loads of electricity, cooling, and heating are selected based on the planning data. The price of electricity, heating, cooling, and gasoline was determined (Ma et al., 2017). Fig. 6 shows the normal daily energy demand load for power, heating, and cooling.

After MEG is linked to the power grids, as shown in Fig. 7, it relations by means of upper energy grids (UEG) for energy sales. Based on the scenario production methods and reduction

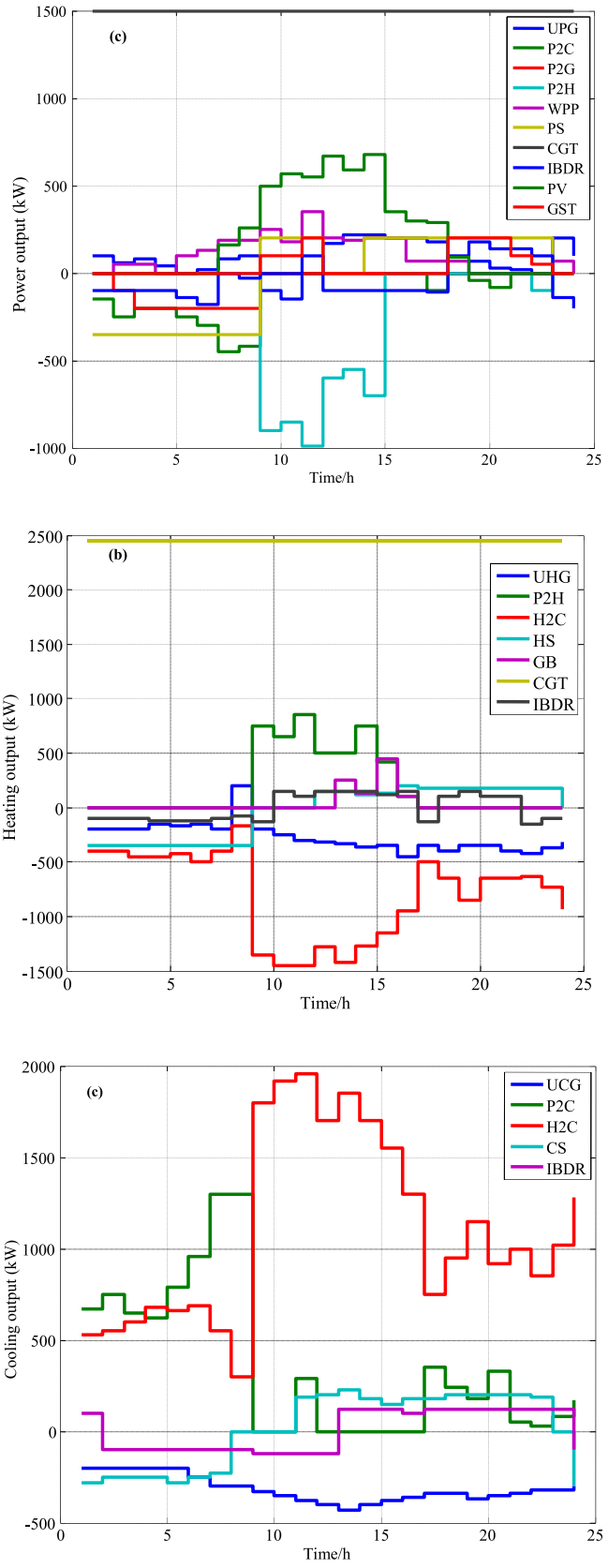

Fig. 16. The optimal results of MEG linked to the upstream power grid.

mentioned in Ju et al. (2019), 10 scenarios are simulated. The scenario with the maximum probability of occurrence is determined

Table 1
The data of the installed energy component.

EP	Output/kW	Price/(¥/kWh)	EC	Output/kW	ES	Capacity/kWh	Output/kW	
							Charge	Discharge
WPP	300	0.57	P2H	1000	PS	1000	200	300
PV	800	0.55	P2C	1000	HS	1000	200	300
CGT	2000	0.48	H2C	1500	CS	1000	300	400
GB	1500	0.24	P2G	150	–	–	–	–

Table 2
PBDR and IBDR parameters for different energy forms.

Type	PBDR						IBDR/(¥/(kW h))	
	Period			Price/(¥/(kW h), ¥/m^3)			Up	Down
	Peak	Flat	Valley	Peak	Flat	Valley		
Power	09:00–11:00&18:00–22:00	12:00–17:00&23:00–24:00	01:00–08:00	0.65	0.4	0.25	0.85	0.25
Heating	1:00–8:00&20:00–24:00	17:00–19:00	09:00–16:00	0.45	0.35	0.25	0.55	0.15
Cooling	11:00–15:00	08:00–10:00&16:00–19:00	01:00–07:00&20:00–24:00	0.4	0.35	0.25	0.45	0.15
Gas	09:00–12:00&18:00–22:00	13:00–17:00	01:00–08:00&23:00–24:00	5.2	3.10	3.50	-	-

Table 3
MEG planning results in the upper-layer model.

	EP/(kW h)				EC/(kW h)				GST	ES/(kW h)			Revenue/¥
	WPP	PV	CGT	GB	P2H	P2G	P2C	H2C		PS	HS	CS	
Power	2725	5311	35 010	–	–	−5037	–	–	793	±2000	–	–	8635
Heating	–	–	53 985	783	3289	–	–	–	–	–	±2000	–	19 658
Cooling	–	–	–	–	–	–	199	29 001	–	–	–	2200,−1800	2696

as the planning data of the day before and the scenario with the most extreme oscillation is determined as real-time planning data. Fig. 8 shows the WPP and PV output in the day before and real-time periods.

Given the demand load distribution, the flat, peak, and valley periods are separated. The elasticity of energy demand price is determined based on Usta et al. (2018). If PBDR is regulated, the heating price change is the same as the price of electricity in different periods. The heating load is reduced by 20% during the peak period. In the other periods, it is increased by 15% and 5%. In Table 2, the PBDR and IBDR parameters are presented for different energy forms.

6.2. Planning results

(A) Scheduled results for the upper layer

This model contains the prediction outputs of day-ahead as input data to maximize the operating revenue. Table 3 shows the MEG planning results in the upper-layer model.

According to the table above, PV, WPP, and CGT are employed to supply energy load. PS and GST are generally used to provide peak-correction services. CGT and P2H are employed to supply heating load. HS is employed to provide heating correction services. The cooling load is met by H2C because the power supply revenue is higher than the P2C revenue. The heating costs are relatively low and the main concern is known to H2C to make the most of revenue. Fig. 9 shows the optimization results of the upper-layer synchronized model.

As shown in Fig. 8, P2G, P2H, and P2C exchange power keen on natural gas, heating, and cooling, respectively, in the valley period, whereas PS supplies electricity in the valley time and discharges it in the peak time. P2H and H2C simultaneously convert power into heating and cooling, respectively, in the peak time.

(B) Planning results for the lower-layer model

The lower-level model essentially consists of two sub-processes from the modified ES and DR planning models. In Table 4, the planning results of different models are presented.

According to Table 4, the efficiencies of PS and HS vary in the range of 400 kWh and CS oscillations vary from 600 kW to 200 kW. ES must bear the cost of energy consumption in the valley period. Therefore, the total revenue is reduced by 479.85. IBDR has been implemented to provide peak-correction services. Compared to the modified ES model, the WPP and PV outputs have increased by 83 kWh and 171 kWh, respectively. The operating revenue increases. Fig. 10 presents the optimized results of the lower layer.

Based on Fig. 10, in the lower layer, IBDR is only planned to provide the positive output power from 6 pm to 9 pm and negative output power at other times. IBDR provides positive or negative heat output with respect to load distribution at the peak valley. IBDR increases demand load by meeting negative cooling output and most of the electricity (usually WPP and PV) is converted into cooling in order to increase operational efficiency. Fig. 11 shows the planning results of MEG with different models.

Based on Fig. 10, when output deviation occurs in the real-time model, WPP and PV outputs should be decreased, especially when the demand load is low such as in the valley time. On the other hand, ES and IBDR can somehow handle this by means of output deviations. In the valley period, the output deviation can be improved by increasing the load, which can flatten the load profile and reduce the extent of changes in the operation efficiency curve.

6.3. Effect of PBDR optimization

PBDR can convert a piece of the peak demand to the valley demand with respect to the cost of time used. The price demand flexibility of different energy forms, and power, cooling, and heating demand after implementation of PBDR can be computed. Fig. 12 presents the demand load and energy cost in different periods after the implementation of PBDR.

Based on Figs. 7 and 12, there are supplementary features surrounded by various models of energy prices, such as cooling and heating supplements. Compared to the load profile before the implementation of PBDR, the energy load graphs of the different models have become flatter due to the increased energy prices

Table 4
Planning results of different models.

	WPP/(kWh)	PV/(kWh)	CGT/(kWh)		ES/(kWh)			IBDR/(kWh)			Revenue/¥
			Power	Heating	Power	Heating	Cooling	Power	Heating	Cooling	
Upper-layer model	2721	5401	35 011	53 921	±2000	±2000	2200–1800	-	-	-	33 954.74
Modified ES model	2439	4898	35 102	53 911	±2400	±2400	±2400	–	–	–	30 468.44
DR planningmodel	2528	5124	35 318	54 568	±2400	±2400	±2400	400–1878	900–1500	100–2300	33 398.87

Table 5
Demand load and operating revenue before and after PBDR.

Scenario	Power		Heating		Cooling		Peak-to-valley ratio		
	Revenue	Cost	Revenue	Cost	Revenue	Cost	Power	Heating	Cooling
Before PBDR	29 479	20 393	22 700	1943	12 234	8686	1.80	2.61	3.21
After PBDR	29 510	14 508	22 728	861	12 222	9014	1.63	2.22	2.74

Table 6
Planning results before and after PBDR (kWh).

Scenario	WPP	PV	GST	CGT		IBDR		
				Power	Heating	Power	Heating	Cooling
Before PBDR	2534	5162	674	35 514	54 610	400, −1896	900, −1500	100, −2300
After PBDR	2614	5329	1042	36 437	54 011	1140, −1200	100, −2310	−2400
Scenario	P2H	GB	HS	PS	P2G	P2C	H2C	CS
Before PBDR	3109	1957	±2400	±2400	−3313	1193	30 217	±2400
After PBDR	7485	35	±2150	±2200	−1537	652	30 865	±2150

in the peak periods and decreased energy prices in the valley periods. Table 5 shows the demand load and operation efficiency before and after implementation of PBDR.

Based on Table 5, if PBDR is evaluated, the peak-to-valley ratio of demand for power, cooling, and heating is decreased significantly. Compared to the results of before the implementation of PBDR, the price of electricity has increased by 135 yuan, while the operation cost has decreased by 5875 yuan. To fully use all parts of the peak, MEG saves energy in the valley time and releases it in the peak time. Cooling is sometimes provided by P2C and H2C. Increasing the price of energy has also increased its fixed price. Figure 13 presents the results of MEG planning after PBDR.

Based on Fig. 13, if PBDR is evaluated, the output of CGT will keep a constant value and PBDR indicates the reduction of the peak load service from CGT. PS and IBDR can provide sufficient services for peak correction. In the valley period, a part of the energy is converted into gas for higher efficiency. P2H employed in the peak time is to eliminate the heating load. In Table 6, P2H notes the planning results before and after the PBDR implementation.

According to the table, if PBDR is evaluated, the PV, WPP, and GST output will increase, but PG energy usage will be reduced. Given the large output of PV and WPP, the heating from P2H will increase, whereas cooling from P2C will decrease. IBDR is implemented for more load cooling. In general, PBDR reduces the need for peak correction, therefore, ES output is reduced. Additionally, PBDR uses energy, heating, and cooling for the uniformity of the demand load curve, so that it could be optimized for the operation of overwhelming energy.

6.4. P2G optimization effect

P2G can convert energy into natural gas which can be used by CGT or GB as a source of energy and heating or sold to the natural gas network. Fig. 14 shows the output of MEG scheduling without P2G.

As shown in Fig. 14, if P2G is not implemented, the power that would have been converted to natural gas will now be converted to heat. Compared to P2G, WPP and PV output are reduced. In Table 7, the MEG planning results with various P2G capacities are presented.

Based on Table 7, P2G can increase the energy transferred into natural gas by P2G. When the evaluated energy from P2G is increased by 442 kW, the total GST output is increased by 1211 kW. On the other hand, a higher capacity of P2G is not necessarily better. When P2G capacity is 145 kW or 280 kW, an increase in P2G output is generally steady. When the P2G capacity is 450 kW, the increase in P2G output is smaller. Fig. 15 shows the optimized P2G-GST outputs with different capacities.

Based on Fig. 15, when the capacity is less than 150 kW, some natural gas is unswervingly sold to the gas network. When the capacity is more than 150 kW, the natural gas produced by P2G is stored in GST and when the value of natural gas is increased, it is given to the natural gas network. When the P2G capacity is more than 300 kW, the energy curves are uniform, which suggests that the P2G capacity has reached its maximum value. When MEG is connected to an upstream grid, the surplus energy can be sold to the upstream grid for economic benefits. Fig. 16 presents the optimal results of MEG connected to the upstream energy grid.

7. Conclusion

To deal with the effect of wind and PV uncertainties on the MEG optimized by the two-stage optimization scheme, the wind and PV energies are used as random variables in order to prepare a high-layer planning model. Moreover, the real output of wind and PV is employed as recognition for random variables to create a planning model for the lower layers. Finally, the artificial bee colony optimization algorithm is developed and proposed to solve the proposed two-stage model. It can be seen that the MEG can use wind and solar energy and natural gas to supply the demand load for power, cooling, and heating. The renewable energy source (RES) power must overcome uncertainty by dividing the scheduled periods on a daily basis at a certain time. After the implementation of PBDR, the peak demand is significantly reduced compared to the valley demand for power, heating, and cooling. The supplementary features for various models of energy prices are employed to make the maximum possible operating

Table 7
MEG planning results with various P2G capacities.

Capacity/kW	WPP/kW h	PV/kW h	CGT/kW h		GST/kW h	GB/kW h	P2G/kW h	P2H/kW h	P2C/kW h	H2C/kW h	Gas/m^3		
			Power	Heating							P2G	CGT	EG
0	2456	5042	34 111	48 355	–	1525	–	7301	570	30 244	–	–	–
75	2456	5042	33 585	53 111	485	351	3985	3464	1045	30 185	324	54	261
150	2523	5161	33 417	53 865	755	400	4975	4954	1064	30 174	405	88	301
300	2585	5252	33 427	53 488	1009	532	5704	2639	1104	30 301	465	128	324
450	2668	5436	33 562	53 289	1232	361	5817	2754	1215	29 955	464	147	315

revenue. Following PBDR, only IBDR and PS are employed to supply the peak reduction service and notice a constant value of energy and heating source in the CGT.

CRediT authorship contribution statement

Muhammad Hammad Saeed: Investigation, Methodology, Writing – review & editing. **Wang Fangzong:** Data curation, Formal analysis. **Sultan Salem:** Resources, Software, Supervision, Writing – review & editing. **Yousaf Ali Khan:** Conceptualization, Validation, Writing – review & editing. **Basheer Ahmad Kalwar:** Preliminary preparation, Validation, Writing – review & editing. **Ashk Fars:** Preliminary preparation, Conceptualization.

Declaration of competing interest

The authors declare that they have no known competing financial interests or personal relationships that could have appeared to influence the work reported in this paper.

References

Ambia, Mir Nahidul, et al., 2014. Power management of hybrid micro-grid system by a generic centralized supervisory control scheme. Sustain. Energy Technol. Assess. 8, 57–65.

Azeem, Omar, et al., 2021. A comprehensive review on integration challenges, optimization techniques and control strategies of hybrid AC/DC Microgrid. Appl. Sci. 11.14, 6242.

Bahramara, Salah, Sheikhahmadi, Pouria, Golpîra, Hêmin, 2019. Co-optimization of energy and reserve in standalone micro-grid considering uncertainties. Energy 176, 792–804.

Elsied, Moataz, et al., 2015. Energy management and optimization in microgrid system based on green energy. Energy 84, 139–151.

Hannan, M.A., et al., 2020. Optimized controller for renewable energy sources integration into microgrid: Functions, constraints and suggestions. J. Clean. Prod. 256, 120419.

Hoang, Anh Tuan, Nguyen, Xuan Phuong, 2021. Integrating renewable sources into energy system for smart city as a sagacious strategy towards clean and sustainable process. J. Cleaner Prod. 127161.

Jadidbonab, Mohammad, Babaei, Ebrahim, Mohammadi-ivatloo, Behnam, 2019. CVaR-constrained scheduling strategy for smart multi carrier energy hub considering demand response and compressed air energy storage. Energy 174, 1238–1250.

Ju, Liwei, et al., 2016. A bi-level stochastic scheduling optimization model for a virtual power plant connected to a wind–photovoltaic–energy storage system considering the uncertainty and demand response. Appl. Energy 171, 184–199.

Ju, Liwei, et al., 2019. A risk aversion optimal model for microenergy grid low carbon-oriented operation considering power-to-gas and gas storage tank. Int. J. Energy Res. 43.10, 5506–5525.

Ju, Liwei, et al., 2020. A two-stage optimal coordinated scheduling strategy for micro energy grid integrating intermittent renewable energy sources considering multi-energy flexible conversion. Energy 196, 117078.

Ju, Liwei, et al., 2021. An interactive dispatching strategy for micro energy grids considering multi-energy flexible conversion based on the three-level optimization perspective. Sustainable Cities Soc. 64, 102504.

Kumar, Abhishek, et al., 2019. Strategic integration of battery energy storage systems with the provision of distributed ancillary services in active distribution systems. Appl. Energy 253, 113503.

Leonori, Stefano, et al., 2020. Optimization strategies for microgrid energy management systems by genetic algorithms. Appl. Soft Comput. 86, 105903.

Li, Zhengmao, Xu, Yan, 2019. Temporally-coordinated optimal operation of a multi-energy microgrid under diverse uncertainties. Appl. Energy 240, 719–729.

Li, Yushuai, et al., 2020. A distributed double-Newton descent algorithm for cooperative energy management of multiple energy bodies in energy internet. IEEE Trans. Ind. Inf. 17.9, 5993–6003.

Lu, Qing, et al., 2020. Optimal household energy management based on smart residential energy hub considering uncertain behaviors. Energy 195, 117052.

Ma, Tengfei, Wu, Junyong, Hao, Liangliang, 2017. Energy flow modeling and optimal operation analysis of the micro energy grid based on energy hub. Energy Convers. Manage. 133, 292–306.

Moghaddas-Tafreshi, Seyed Masoud, et al., 2019. Optimal energy management of a grid-connected multiple energy carrier micro-grid. Appl. Therm. Eng. 152, 796–806.

Mohseni, Soheil, et al., 2021. Strategic design optimisation of multi-energy-storage-technology micro-grids considering a two-stage game-theoretic market for demand response aggregation. Appl. Energy 287, 116563.

Sun, Liling, et al., 2020. A modified surrogate-assisted multi-swarm artificial bee colony for complex numerical optimization problems. Microprocess. Microsyst. 76, 103050.

Usta, Ilhan, et al., 2018. A new estimation approach based on moments for estimating Weibull parameters in wind power applications. Energy Convers. Manage. 164, 570–578.

Wang, Ran, et al., 2014. Power demand and supply management in microgrids with uncertainties of renewable energies. Int. J. Electr. Power Energy Syst. 63, 260–269.

Wang, Luhao, et al., 2017. Integrated scheduling of energy supply and demand in microgrids under uncertainty: A robust multi-objective optimization approach. Energy 130, 1–14.

Wang, Yongli, et al., 2019. Planning and operation method of the regional integrated energy system considering economy and environment. Energy 171, 731–750.